



Moraine crest or slope: An analysis of the effects of boulder position on cosmogenic exposure age

DOI:

[10.1016/j.epsl.2021.117092](https://doi.org/10.1016/j.epsl.2021.117092)

Document Version

Accepted author manuscript

[Link to publication record in Manchester Research Explorer](#)

Citation for published version (APA):

Tomkins, M. D., Dortch, J. M., Hughes, P., Huck, J. J., Pallàs, R., Rodés, Á., Allard, J. L., Stimson, A. G., Bourlès, D., Rinterknecht, V., Jomelli, V., Rodríguez-Rodríguez, L., Copons, R., Barr, I. D., Darvill, C. M., & Bishop, T. (2021). Moraine crest or slope: An analysis of the effects of boulder position on cosmogenic exposure age. *Earth and Planetary Science Letters*, 570, [117092]. <https://doi.org/10.1016/j.epsl.2021.117092>

Published in:

Earth and Planetary Science Letters

Citing this paper

Please note that where the full-text provided on Manchester Research Explorer is the Author Accepted Manuscript or Proof version this may differ from the final Published version. If citing, it is advised that you check and use the publisher's definitive version.

General rights

Copyright and moral rights for the publications made accessible in the Research Explorer are retained by the authors and/or other copyright owners and it is a condition of accessing publications that users recognise and abide by the legal requirements associated with these rights.

Takedown policy

If you believe that this document breaches copyright please refer to the University of Manchester's Takedown Procedures [<http://man.ac.uk/04Y6Bo>] or contact uml.scholarlycommunications@manchester.ac.uk providing relevant details, so we can investigate your claim.



1 **Moraine crest or slope: an analysis of the effects of**
2 **boulder position on cosmogenic exposure age**

3 **Matt D. Tomkins^{1,2}, Jason M. Dortch³, Philip D. Hughes^{1,2}, Jonny J. Huck¹, Raimon**
4 **Pallàs⁴, Ángel Rodés⁵, James L. Allard^{1,2}, Andrew G. Stimson¹, Didier Bourlès⁶,**
5 **Vincent Rinterknecht⁶, Vincent Jomelli⁶, Laura Rodríguez-Rodríguez⁷, Ramon**
6 **Copons⁸, Iestyn D. Barr^{9,2}, Christopher M. Darvill^{1,2}, Thomas Bishop¹**

7 ¹Department of Geography, University of Manchester, Manchester, M13 9PL, UK

8 ²Cryosphere Research at Manchester, Manchester, UK

9 ³Kentucky Geological Survey, University of Kentucky, Lexington, USA

10 ⁴Departament de Dinàmica de la Terra i de l'Oceà, Universitat de Barcelona, 08028 Barcelona, Spain

11 ⁵Scottish Universities Environmental Research Centre, Rankine Avenue, East Kilbride G75 0QF, UK

12 ⁶Aix-Marseille Univ., CNRS, IRD, INRA, Coll France, UM 34 CEREGE, Technopôle de l'Environnement
13 Arbois-Méditerranée, BP80, I 3545 Aix-en-Provence, France

14 ⁷Dpto. Ciencias de la Tierra y Física de la Materia Condensada, Universidad de Cantabria, Avenida de los
15 Castros s/n, 39005 Santander, Spain

16 ⁸Snow and Mountain Research Centre of Andorra (CENMA), Andorran Research Institute (IEA), Sant
17 Julià de Lòria, Andorra

18 ⁹Department of Natural Sciences, Manchester Metropolitan University, Manchester, UK

19 **Keywords**

20 Cosmogenic nuclides

21 Moraine

22 Geologic uncertainty

23 Degradation

24 Weathering

25 Schmidt hammer

26 **Abstract**

27 Terrestrial cosmogenic nuclide dating of ice-marginal moraines can provide unique insights
28 into Quaternary glacial history. However, pre- and post-depositional exposure histories of
29 moraine boulders can introduce geologic uncertainty to numerical landform ages. To avoid
30 geologic outliers, boulders are typically selected based on their depositional context and
31 individual characteristics but while these criteria have good qualitative reasoning, many have
32 not been tested quantitatively. Of these, boulder location is critical, as boulders located on
33 moraine crests are prioritised, while those on moraine slopes are typically rejected. This
34 study provides the first quantitative assessment of the relative utility of moraine crest and
35 moraine slope sampling using new and published ^{10}Be and ^{36}Cl ages ($n = 19$) and Schmidt
36 hammer sampling (SH; $n = 635$ moraine boulders, $\sim 19,050$ SH R -values) in the northern and
37 southern Pyrenees. These data show that for many of the studied moraines, the spatial
38 distribution of “good” boulders is effectively random, with no consistent clustering on
39 moraine crests, ice-proximal or -distal slopes. In turn, and in contrast to prior work, there
40 is no clear penalty to either moraine crest or moraine slope sampling. Instead, we argue that
41 landform stability exerts a greater influence on exposure age distributions than the
42 characteristics of individual boulders. For the studied landforms, post-depositional stability is
43 strongly influenced by sedimentology, with prolonged degradation of matrix-rich
44 unconsolidated moraines while boulder-rich, matrix-poor moraines stabilised rapidly after
45 deposition. While this pattern is unlikely to hold true in all settings, these data indicate that

46 differences between landforms can be more significant than differences at the intra-landform
47 scale. As ad hoc assessment of landform stability is extremely challenging based on
48 geomorphological evidence alone, preliminary SH sampling, as utilised here, is a useful
49 method to assess the temporal distribution of boulder exposure ages and to prioritise
50 individual boulders for subsequent analysis.

51 **I. Introduction**

52 Ice-marginal moraines are classic features of glaciated mountain ranges and are prominent
53 terrestrial records of glacial history (Hallet and Putkonen, 1994). By constraining the timing
54 of moraine deposition, it is possible to reconstruct the growth and decay of glaciers and ice
55 sheets through the Quaternary and the palaeoclimatic drivers of glacial cycles. Recent
56 developments in terrestrial cosmogenic nuclide (TCN) dating have transformed our
57 understanding of Quaternary glaciations by permitting direct analysis of the fragmentary
58 glacial stratigraphic record (Zreda and Phillips, 1995). Despite this progress, TCN dating can
59 be complicated by geologic processes which result in pre- or post-depositional exposure of
60 rock surfaces and which account for apparent TCN ages that pre- or post-date the assumed
61 age of the landform (Applegate et al., 2010). Of these, post-depositional erosion,
62 exhumation and shielding have been shown to profoundly influence TCN age distributions
63 (Briner et al., 2005; Zech et al., 2005; Heyman et al., 2011; Stübner et al., 2017; Chevalier
64 and Replumaz, 2019).

65 To avoid geologic outliers, researchers select samples based on the depositional context
66 and characteristics of individual surfaces. Previous studies have advocated sampling:

- 67 • boulders on moraine crests or on flat, stable surfaces (Gosse et al., 1995),

- 68 • the tallest boulders, to minimise the likelihood of post-depositional shielding
69 (Heyman et al., 2016),
- 70 • the largest boulders or boulders embedded in the moraine matrix (Ivy-Ochs et al.,
71 2007), to minimise the likelihood of post-depositional instability,
- 72 • well-rounded boulders which preserve evidence of glacial transport (Darvill et al.,
73 2015), to minimise the likelihood of pre-depositional exposure.

74 However, while these criteria have good qualitative reasoning, many have not been tested
75 quantitatively. In turn, further work is required to test existing criteria for sample selection
76 and to develop quantitative methods which minimise the effects of geologic processes
77 (Dortch et al., 2013; 2021). These developments have the potential to significantly improve
78 the robustness of TCN datasets and the chronological utility of the moraine record
79 (Applegate et al., 2012). Within this context, this paper focuses on a fundamental
80 component of TCN sample selection; the effect of moraine crest sampling on boulder
81 exposure age. Of the above criteria, boulder location is critical, as boulders on moraine
82 crests are prioritised, while those on moraine slopes are typically rejected, irrespective of
83 their individual characteristics.

84 While this approach is qualitatively sound, early numerical models of moraine evolution
85 predicted the greatest ground-lowering at moraine crests (Hallet and Putkonen, 1994;
86 Putkonen and Swanson, 2003) with a period of maximum instability as glaciers retreat and as
87 oversteepened ice-proximal slopes erode and stabilise (Porter and Swanson, 2008).

88 However, moraines continue to degrade through time as a function of moraine height and
89 sedimentology (Putkonen and Swanson, 2003; Putkonen et al., 2008; Schaller et al., 2009), as
90 diffusive processes remove fine-grained material from moraine crests and deposit material at
91 the base of moraine slopes (Applegate et al., 2010). Over time, these processes drive

92 exhumation of boulders which have been shielded from cosmogenic exposure. In turn, the
93 age distribution of moraine crest boulders may primarily reflect an initial stabilisation phase
94 (~1 ka; Briner et al., 2005; Dortch et al., 2010), modified by the ongoing process of moraine
95 degradation, rather than the timing of initial moraine deposition. In contrast, slope diffusion
96 models and lichenometric methods predict relative stability on moraine slopes (Hallet and
97 Putkonen, 1994; Putkonen and O'Neil, 2006), but these are rarely sampled for TCN, in part
98 due to the perceived risk that boulders may rotate, shift or roll throughout the lifetime of
99 the moraine. This dichotomy between model predictions and sampling procedures raises a
100 fundamental and currently unanswered question: should moraine crests or moraine slopes
101 be prioritised in TCN sample selection?

102 To address this uncertainty, we utilise 19 new and published ^{10}Be and ^{36}Cl TCN ages and
103 635 Schmidt hammer calibrated-exposure ages (SH; 19,050 SH *R*-values) from ice-marginal
104 moraines in the northern and southern Pyrenees. Weathering-based analyses are utilised
105 here to enable intensive sampling of boulders across the moraine surface, with results
106 verified against independent TCN ages. In total, these data provide the first quantitative
107 assessment of the relative utility of moraine crest and moraine slope sampling.

108 **2. Methods**

109 **2.1. Moraine selection**

110 Six moraines of varying age, geomorphology and sedimentology were selected in the
111 Pyrenees (Fig. 1); a mountain range which was extensively glaciated during Pleistocene cold
112 stages (see Fig. 1F; Calvet et al., 2011). Moraines were selected to encompass the primary
113 deglaciation phases of the Pyrenees since the global Last Glacial Maximum (LGM) and all
114 feature large populations of quartz-rich granitic moraine boulders, sourced from Axial zone

115 granite outcrops in the Arànsers, Gave de Pau and Noguera Rigaborçana glaciated valleys
116 (Fig. 1E), and which are suitable for ^{10}Be dating. While this focused approach does not
117 comprise all moraine types or depositional settings, these sites do encompass a range of
118 moraine types commonly found in cirque and valley landsystems and which are often
119 priority targets for TCN dating (i.e. \leq LGM).

120 Selected moraines include both left (north) and right (south) latero-frontal moraines in the
121 Arànsers catchment, Cerdanya (Fig. 2A). These moraines are matrix-rich (matrix-supported),
122 steep-sided ($30\text{--}40^\circ$), heavily forested (Mountain pine: *Pinus uncinata*), and record the
123 maximum ice extent of the Arànsers glacier during the Würmian cold stage (110 – 11.7 ka;
124 Calvet et al., 2011). The right latero-frontal moraine has previously been dated using ^{36}Cl (n
125 = 2; Palacios et al., 2015). To supplement these data, a further 10 boulders were selected
126 for ^{10}Be analysis (Table 1). Methods used for sample preparation, ^{10}Be measurement and
127 exposure age calculation are detailed in the Supplementary Information.

128 On the north side of the Pyrenees, matrix-rich lateral moraines were selected in the Gave
129 de Pau catchment (Fig. 2B). At least two neighbouring (~ 60 m) but distinct lateral moraine
130 ridges have been identified (Soum d'Ech moraines; Fig. 1D), with the outer moraine
131 previously dated using ^{10}Be ($n = 4$; Rodés, 2008). As at Arànsers, these moraines likely
132 correspond to the Würmian MIE but their distinctive morphologies (multiple nested ridges
133 vs. a single large moraine) likely reflects a topographic control on moraine deposition (open
134 topography vs. confined valley; Barr and Lovell, 2014; Palacios et al., 2015).

135 On the south side of the Pyrenees, and in the Val de Molières catchment of the Noguera
136 Rigaborçana, sampled sites include the boulder-rich (clast-supported), matrix-poor Outer
137 Pleta Naua terminal moraine (Fig. 3B, 1B), previously assigned to Greenland Stadial I based
138 on ^{10}Be ($n = 3$; Pallàs et al., 2006), and the Tallada cirque moraine (Fig. 3A, 1A), which

139 consists of a single sharp-crested, arcuate terminal moraine with two minor ice-proximal
140 ridges. Both the Outer Pleta Naua and Tallada moraines are primarily composed of wedged
141 angular boulders, with little or no sediment matrix. Although undated, the Tallada moraine
142 is assumed to be late-Holocene in age, as evidenced by minimal boulder weathering (Pallàs
143 et al., 2006), while its elevation (~2400 m), topographic setting (enclosed cirque; ~0.16 km²)
144 and aspect (NNE) likely contribute to the inter-annual preservation of a small snowfield
145 (~0.03 km²). These factors may have enabled glacier growth or re-advance during more
146 recent climatic periods (e.g. the Little Ice Age).

147 **2.2. Sampling approach**

148 To investigate the depositional and post-depositional histories of these moraines, glacial
149 boulders were selected to cover the entire moraine surface, including the moraine crest
150 (C), the inner ice-proximal slope (IS) and the outer ice-distal slope (OS), while the number
151 of selected boulders varied as a function of moraine size ($n = 60 - 275$). In turn, boulder
152 selection was primarily motivated by spatial location and the construction of a dense matrix
153 of sampling points, rather than individual boulder characteristics. Each boulder was sampled
154 using an N-type Schmidt hammer (SH) to assess the relative degree of weathering following
155 the sampling approach of Tomkins et al. (2018a). All boulders were of sufficient size (> 25
156 kg; Sumner and Nel, 2002) and sampled areas were free of surface discontinuities (Williams
157 and Robinson, 1983) and lichen (Matthews and Owen, 2008). Thirty *R*-values were recorded
158 for each boulder by a single operator and no outliers were removed following Niedzielski et
159 al. (2009). Schmidt hammer functioning was assessed regularly using the manufacturer's test
160 anvil, with instrument and age calibration performed following Tomkins et al. (2018a). In
161 total, 635 moraine boulders were sampled across the selected sites and 19,050 SH *R*-values
162 were generated. To compliment these data, the dimensions, surface features and

163 depositional context of each sampled boulder were recorded (see Supplementary
164 Information).

165 Schmidt hammer *R*-values correspond to the degree of surface weathering, assuming
166 minimal lithological variation between tested rock surfaces (McCarroll, 1989), and are
167 inversely proportional to surface exposure age. The rate and style of weathering may also
168 be modified by climate (Riebe et al., 2004; Portenga and Bierman, 2011; Marrero et al.,
169 2018). At the intra-landform scale, lithologic-climatic variability is absent as all sampled
170 boulders share a common source area and climatic regime. At the inter-landform scale,
171 variability in rock type is minimal, as all sampled boulders were coarse- to medium-grained
172 granites and granodiorites. Finally, while regional climatic variability could account for
173 variability in weathering rates across the studied sites, previous work has shown that rates
174 of sub-aerial weathering of granite are consistent over large spatial scales for regions of
175 similar climate (Tomkins et al., 2018b).

176 **2.3. Calculating SH-calibrated exposure ages**

177 As granitic lithologies have proved effective for calibrated-relative age dating, SH *R*-values
178 are used here as a proxy for exposure age based on a ¹⁰Be-SH calibration dataset developed
179 by Tomkins et al. (2018b). This dataset comprises 52 ¹⁰Be ages, distributed between 4.2 ±
180 0.3 ka and 51.8 ± 4.5 ka (Fig. 4), obtained from granite and granodiorite glacial boulders and
181 glacially-sculpted bedrock from across the central and eastern Pyrenees and their
182 corresponding SH *R*-values (Tomkins et al., 2018b). This dataset has been updated to include
183 two additional ¹⁰Be dated surfaces from the Val de Molières (MUL01 and MUL03; Pallàs et
184 al., 2006; see Supplementary Table 1).

185 To utilise these data, ¹⁰Be ages were recalculated using the CRONUS Earth Web Calculator
186 (Version 2.0; Marrero et al., 2016, available at: <http://cronus.cosmogenicnuclides.rocks/2.0/>,

187 accessed: 01/09/2020), relative to the production rate dataset in Borchers et al. (2016) and
188 the time-dependent L_m scaling scheme (Lal, 1991; Stone, 2000), and assuming 0 mm ka^{-1}
189 erosion. Recalculated ^{10}Be ages are minimum estimates, as no corrections were made for
190 shielding by snow, sediment or vegetation, surface erosion, or isostatic adjustment. To
191 ensure consistency, all ^{10}Be and ^{36}Cl TCN ages discussed in this paper have been
192 recalculated using these input parameters. This includes published ages from Pallàs et al.
193 (2006), Rodés (2008), and Palacios et al. (2015), in addition to the 10 new ^{10}Be dated
194 samples from the Arànsér catchment. Full sample details used for exposure age calculation
195 are provided in the Supplementary Information.

196 In turn, a ^{10}Be -SH calibration curve was constructed using logarithmic orthogonal distance
197 regression (ODR, Boggs and Rogers, 1990) which minimises orthogonal residuals to account
198 for measurement uncertainties in both the independent and dependent variables. We utilise
199 Monte Carlo simulations to explicitly incorporate measurement errors; an approach which
200 is preferable to a weighted ODR which requires unnecessary assumptions regarding
201 weighting constants and is biased by TCN age-uncertainty collinearity (Ivy-Ochs et al., 2007;
202 Dortch et al., 2021). Our analytical procedure, which returns prediction estimates (1σ) of \pm
203 $2.0 - 2.3 \text{ ka}$, is described fully in the Supplementary Information and has been implemented
204 in SHED-Earth (<http://shed.earth>), an online calculator developed to enable wider and more
205 consistent application of our approach (Tomkins et al., 2018a). To assess the accuracy of the
206 ^{10}Be -SH calibration curve, 15 ^{10}Be and ^{36}Cl ages from the studied moraines were located and
207 re-sampled with the SH.

208 Based on this calibration curve, mean R -values from the 635 sampled boulders were
209 converted into “SH-calibrated exposure ages” through interpolation. While uncertainty
210 estimates for individual SH-calibrated exposure ages are larger than typical uncertainties

211 associated with individual TCN exposure ages, landform age estimates can be of comparable
212 precision to established techniques when derived from large SH datasets (e.g. n boulders \geq
213 30; Tomkins et al., 2018b) and when appropriate statistical approaches for outlier
214 identification and error propagation are employed (Applegate et al., 2012; Dortch et al.,
215 2013; 2021).

216 **2.4. Calculating landform ages**

217 To determine the timing of moraine deposition at each site, we analysed the distribution of
218 SH-calibrated exposure ages using the Probabilistic Cosmogenic Age Analysis Tool (P-CAAT
219 Version 1.0; Dortch et al. 2021). This method builds on the earlier work of Dortch et al.
220 (2013) and utilises non-linear curve fitting and a Monte Carlo style approach to isolate
221 component Gaussian distributions to account for positive (prior exposure) and negative
222 skew (incomplete exposure) of age datasets. The results of this analysis are presented in Fig.
223 5 and Table 2. To assess the validity of these landform ages, we compared these data to the
224 distribution of ^{10}Be and ^{36}Cl ages from the studied landforms (Table 1; Pallàs et al., 2006;
225 Rodés, 2008; Palacios et al., 2015).

226 Based on landform age analysis, individual boulders were sorted into “good” and “bad”
227 groups, which are defined by the 2σ (95%) age boundaries of the calculated landform age.
228 Boulders which returned SH-calibrated exposure ages within 2σ of the landform age were
229 classed as “good”, while those younger or older than the landform age ($> 2\sigma$) were classed
230 as “bad”. Selection of a broad 2σ threshold is appropriate given the measurement
231 uncertainties associated with SH sampling, in addition to the systematic and geologic
232 uncertainties inherited from TCN dating. Logistic analysis is used to distinguish boulders
233 which correspond to the timing of moraine deposition or initial stabilisation (“good”) from
234 those which are likely compromised by pre- or post-depositional exposure (“bad”).

235 **2.5. Spatial analysis**

236 The spatial distribution of “good” and “bad” boulders was analysed using global and local
237 Moran’s *I* spatial autocorrelation and based on a row-standardised distance-band weights
238 matrix, where the distance band threshold is the minimum distance required to ensure that
239 each boulder has at least two neighbours (Table 3). The Python implementation is available
240 on GitHub: <https://github.com/matt-tomkins/moraine-crest-or-slope>. At the global level,
241 Moran’s *I* was used to assess whether the overall clustering of the data was significantly
242 different from a random distribution. For datasets that are non-random ($p < 0.05$), local
243 Moran’s *I* was used to identify the location of statistically significant boulder clusters (Fig. 6).
244 Current sampling approaches are based on the qualitatively-sound but quantitatively-
245 untested assumptions that (i) the distribution of “good” boulders is non-random, and that
246 (ii) “good” clusters are more likely on moraine crests. These assumptions can be explicitly
247 tested for the studied moraines using global and local Moran’s *I* respectively.

248 **2.6. Sensitivity Analysis**

249 The above analyses provide important information on the relative occurrence and spatial
250 clustering of “good” and “bad” boulders for moraines of varying age and morphology.
251 However, this logistic classification is ultimately dependent on the calculated landform age,
252 which will vary depending on the choice of numeric bandwidth estimator and the size and
253 clustering of the input dataset (Dortch et al., 2021).

254 To evaluate the reproducibility of our results, sensitivity testing was performed to evaluate
255 the number of samples required to reproduce the estimated landform age based on 1σ and
256 2σ thresholds. The full analytical approach is described in the Supplementary Information
257 and the results are presented in Fig. 7B.

258 **3. Results**

259 **3.1. SH-calibrated exposure ages**

260 There is a strong correlation between recalculated ^{10}Be ages and their corresponding SH R -
261 values (Fig. 4; $n = 54$). Moreover, of the 15 ^{10}Be and ^{36}Cl dated boulders re-sampled with the
262 SH, the majority closely match the existing calibration dataset ($n = 13$). These observations
263 indicate that when lithological variation is minimised, the relative degree of rock surface
264 weathering can be used as a proxy for surface exposure age.

265 Exceptions to this correlation are samples ECH03 (17.2 ± 3.5 ka) and ECH04 (16.8 ± 3.3
266 ka) from the Soum d'Ech moraines (Rodés, 2008) which are significantly more weathered
267 ($\sim 38 R$) than their corresponding ^{10}Be ages would predict ($\sim 47 R$). This difference likely
268 reflects sub-surface weathering prior to boulder exhumation. However, the scale of this
269 influence is unlikely to be universal given the close correspondence between sample ECH01
270 (19.7 ± 3.6 ka) and the existing calibration dataset (see Fig. 4). While sub-surface weathering
271 of boulders under thin soil cover (~ 25 cm) can occur (Darmody et al., 2005), boulders are
272 often protected from weathering by sediment burial, as evidenced by the emergence of
273 unweathered boulders from glacial tills and alluvium (Ehlmann et al. 2008). In turn, as SH-
274 calibrated exposure ages from the Soum d'Ech moraines may well incorporate the effects of
275 both sub-aerial and sub-surface weathering, and could also be influenced by weathering rate
276 variability (e.g. differences between the Atlantic- (wet) and Mediterranean-influenced (dry)
277 Pyrenees), it is possible that the estimated depositional age is an overestimate.

278 **3.2. Landform ages**

279 Landform ages derived from SH-calibrated exposure ages and associated P-CAAT model
280 parameters are reported in Table 2 (Dortch et al. 2021). Based on this approach, latero-

281 frontal moraines in the Arànsér catchment were deposited at 23.3 ± 1.1 ka (left) and $22.3 \pm$
282 0.9 ka (right). As these estimates are consistent within measurement uncertainties, and given
283 the comparable morpho-stratigraphy of these deposits (Fig. 2A), we consider moraine
284 deposition to be contemporaneous. No independent dating evidence is available for the left
285 lateral moraine, but 12 TCN ages are now available for the right lateral moraine (^{36}Cl , $n = 2$;
286 ^{10}Be , $n = 10$). Using P-CAAT and selecting the oldest component Gaussian distribution that
287 contains ≥ 3 ages to represent the age of the landform (see Fig. 3 in Dortch et al. 2013),
288 these data return a landform age of 21.5 ± 2.2 ka (Mean bandwidth estimator; Numeric
289 bandwidth = 0.8108, $R^2 = 0.9997$, $p < 0.01$), while the oldest sample is 22.4 ± 1.8 ka (SAL-
290 10). Both estimates are consistent within measurement uncertainties with the SH-derived
291 landform ages.

292 In the Gave de Pau catchment, SH-calibrated exposure ages from the proximal Soum d'Ech
293 lateral moraines return landform ages of 26.2 ± 2.5 ka (outer, $n = 61$) and 26.1 ± 1.7 ka
294 (inner, $n = 39$). While these moraines are morpho-stratigraphically distinct, they cannot be
295 statistically distinguished. It is possible that moraine deposition occurred within the
296 resolution of our sampling approach, or that differences in moraine age have been masked
297 by moraine stabilisation, degradation or sub-surface boulder weathering. As the temporal
298 distribution of SH-calibrated exposure ages is near identical (Table 2), we assign these
299 deposits a landform age of 27.3 ± 1.8 ka based on P-CAAT ($n = 100$; STD / IQR bandwidth
300 estimator; Numeric bandwidth = 0.9877, $R^2 = 0.9989$, $p < 0.01$), and perform subsequent
301 analyses on the combined dataset for computational ease.

302 While this estimate is significantly older than the corresponding ^{10}Be ages (16.8 ± 3.3 ka,
303 17.2 ± 3.5 ka, 19.7 ± 3.6 ka; Rodés, 2008), it is consistent with limiting ^{14}C ages obtained
304 from a proximal palaeolake sediment sequence at Lac de Lourdes (Reille and Andrieu,

305 1995). While the oldest radiometric ^{14}C ages from this over-deepened glacial basin are now
306 considered suspect due to contamination from mineral carbon (Pallàs et al., 2006), a
307 younger AMS ^{14}C age from glaciolacustrine clays suggests initial ice-free conditions by $24.1 \pm$
308 0.4 ka cal. BP (20.025 ± 0.175 ka BP; Sample depth = 920 – 960 cm), as calculated using
309 IntCal 13 (Reimer et al., 2013), while an AMS ^{14}C age from an overlying organic rich layer
310 (gyttja) indicates the culmination of glaciolacustrine sedimentation and deglaciation of the
311 lower Gave de Pau by 18.8 ± 0.3 ka cal. BP (15.460 ± 0.150 ka BP; Sample depth = 740 –
312 750 cm; Reille and Andrieu, 1995). Based on these data, the younger ^{10}Be ages from Soum
313 d’Ech can be considered suspect. Continued glacial occupation of the Soum d’Ech site until
314 ~ 19.7 ka, as inferred from the oldest ^{10}Be age (ECH01; 19.7 ± 3.6 ka), appears unlikely given
315 initial deglaciation of low ground by ~ 24.1 ka. Instead, it appears likely that the ECH samples
316 are representative of final moraine stabilisation, rather than initial deposition. This
317 interpretation is supported by sensitivity analysis (see Section 3.5), as the number of TCN
318 ages ($n = 3$) is below the threshold required to consistently reproduce the landform age
319 derived from the full dataset at 2σ ($n = 11$) and 1σ ($n = 41$).

320 In the Val de Molières catchment of the Noguera Rigaborçana, recalculated ^{10}Be ages on the
321 Outer Pleta Naua moraine range from 12.6 ± 1.5 ka to 13.2 ± 1.6 ka ($n = 3$; Pallàs et al.,
322 2006). These estimates are consistent with the SH-calibrated exposure ages, which range
323 from 11.8 ± 2.0 ka to 13.1 ± 2.0 ka ($n = 60$). As the SH-calibrated exposure ages conform to
324 a normal distribution (Fig. 5B; Shapiro-Wilk test, $W = 0.96$, $p = 0.07$), are well-clustered
325 (IQR = 0.6 ka), and return an excellent P-CAAT model fit with a single component Gaussian
326 ($R^2 = 1$, $p < 0.01$), we use the arithmetic mean (\bar{x}) to represent the age of the landform and
327 estimate the total uncertainty (t) following Dortch et al. (2021) as follows:

328
$$t = \sqrt{SU^2 + GU^2}$$

329 where systematic uncertainty (SU) incorporates measurement errors:

$$330 \quad SU = \frac{\sqrt{\text{Sum of the squared errors}}}{\text{Number of observations}}$$

331 and where geologic uncertainty (GU) incorporates the clustering of the dataset, which is
332 typically interpreted as the effects of pre- and post-depositional processes that modify
333 cosmogenic nuclide concentrations:

$$334 \quad GU = \text{Standard deviation}$$

335 In turn, the Outer Pleta Naua moraine was likely deposited at 12.5 ± 0.4 ka. Applying the
336 same analytical approach ($\bar{x} \pm t$) to the corresponding ^{10}Be ages produces 12.9 ± 1.0 ka,
337 which is statistically indistinguishable. Moreover, these estimates are stratigraphically
338 consistent with independent landform ages in the Val de Molières catchment (Pallàs et al.,
339 2006), with maximum and minimum limiting ages for moraine deposition provided by
340 samples from the Molières (MUL01 = 14.9 ± 2.6 ka, MUL03 = 14.9 ± 1.9 ka) and Inner Pleta
341 Naua moraines respectively (Fig. 3B; IPN01 = 6.3 ± 0.9 ka; Pallàs et al., 2006).

342 Finally, the Tallada cirque moraine returned a landform age of 3.2 ± 0.7 ka. While this SH-
343 derived estimate cannot be independently verified, the limited weathering of the moraine
344 boulders (SH $R \geq 60$), in combination with the topographic setting of the Tallada cirque,
345 appears consistent with a late-Holocene origin.

346 **3.3. Temporal distribution**

347 Estimated landform ages are generally consistent with independent TCN ages ($n = 19$) but
348 the age distribution of SH-calibrated exposure ages varies significantly between the sampled
349 moraines (Fig. 5). For the Arànsér and Soum d'Ech moraines, the distribution of SH-
350 calibrated exposure ages is strongly negatively skewed (Table 2), in line with exhumation

351 models (Applegate et al., 2012), while Tallada is normally distributed with a slight positive
352 skew (Shapiro-Wilk test, $W = 0.98$, $p = 0.56$); a trend which may reflect prior exposure or
353 reworking of glacial material (Applegate et al., 2010).

354 In light of these trends, the proportion of “good” and “bad” boulders, as defined by the 2σ
355 age boundaries of the corresponding landform age, varies between the sampled moraines.
356 The proportion of “good” boulders is highest on the Outer Pleta Naua moraine (100%) and
357 lowest on the Arànsers left (56%) and Arànsers right moraines (49%). For moraines
358 corresponding to the ~gLGM, most “bad” boulders are younger than the assumed age of
359 deglaciation (Table 2), while the Holocene Tallada moraine contains a small but significant
360 component of boulders which are older than the assumed age of deglaciation (14%). Logistic
361 analysis indicates that boulder characteristics (e.g. boulder height) did not have a consistent
362 statistically significant effect on the distribution of “good” and “bad” boulders across the
363 sampled moraines (see Supplementary Information).

364 **3.4. Spatial distribution**

365 Summary statistics for spatial analysis are presented in Table 3. This approach reveals
366 marked inter-landform variation, with statistically significant spatial clustering absent from
367 the Tallada, Outer Pleta Naua and Arànsers right moraines (simulated $p > 0.05$). In turn, the
368 spatial distribution of “good” and “bad” boulders for these moraines is effectively random.

369 One exception to this rule is the Arànsers left moraine where statistically significant
370 clustering is evident (simulated $p < 0.05$) and where clusters identified using local Moran's I
371 have plausible geomorphological explanations (Fig. 6A). Clusters of “young” boulders occur:

- 372 (i) at the moraine terminus,
- 373 (ii) where the moraine crest has been cross-cut and incised by a minor stream and,

374 (iii) where boulders have accumulated at the base of the moraine slope.

375 Additional clusters are also evident on the ice-proximal slope (Fig. 6A). Clusters (i) and (ii)
376 are likely fluvial in origin, with the former explained by incision of the terminal deposits,
377 which may have led to degradation of the lateral flanks and exhumation of moraine
378 boulders. This pattern of post-depositional degradation matches the spatial clustering of ^{36}Cl
379 ages on a comparable gLGM moraine deposited in the nearby Duran valley (see Fig. 11 in
380 Palacios et al., 2015). The second cluster may be partially explained by meltwater erosion,
381 given the proximity of the incised area to the former terminus of the Setut glacier (Fig. 2A).
382 The origins of the remaining “young” clusters are less clear, but these ultimately reflect
383 instability of the ice-proximal slope, although it is not yet clear whether this was driven by
384 autogenic moraine stabilisation or external factors (e.g. subsequent glacial advance, fluvial
385 erosion). Clusters of “good” boulders were also identified on the Arànsér left moraine but
386 these are distributed across moraine crests and ice-proximal and -distal slopes and follow
387 no clear spatial pattern. Finally, local Moran’s *I* identified both “young” and “good” clusters
388 on the outer Soum d’Ech moraine (Fig. 6B) but there is no clear geomorphological evidence
389 which explains their distribution.

390 The proportion of “good” boulders varies markedly between the studied moraines, but this
391 overall trend is relatively consistent across boulder groups (C, IS, OS) at the intra-landform
392 scale (Fig. 7A). While there are clear differences between boulder groups at the Arànsér left
393 and right moraines, there are no consistent trends at the inter-landform scale and no single
394 boulder group performs optimally across all landforms.

395 **3.5. Sensitivity results**

396 Based on the sensitivity analysis described in Section 2.6, there are clear differences in the
397 number of SH samples required to reproduce the landform ages obtained from the full

398 datasets ($n = 60 - 275$; Fig 7B). The Outer Pleta Naua landform age requires only three
399 samples at both 1σ and 2σ . Landform ages for both the Arànsers left and right moraines can
400 be reproduced with relatively few samples at both 1σ ($n \leq 26$) and 2σ ($n \leq 16$), while both
401 the Soum d'Ech and Tallada moraines require ≥ 40 samples to reproduce the landform age
402 at 1σ .

403 These trends are largely explained by the degree of overlap between component Gaussian
404 distributions (see Fig. 5). Both the Tallada (Fig. 5A) and Soum d'Ech moraines (Fig. 5E)
405 feature lower probability component Gaussians, centred on 4.7 ± 0.9 ka and 24.4 ± 1.7 ka
406 respectively, which overlap with the highest probability component Gaussian. In contrast,
407 there is minimal overlap between component Gaussians for the Arànsers left moraine (Fig.
408 5C), despite the high degree of dataset skew and the large number of "bad" boulders (44%).
409 The Arànsers right moraine is intermediate in character (Fig. 5D), with clear unidirectional
410 skew but a greater degree of overlap between the highest probability Gaussian (22.3 ± 0.9
411 ka) and younger lower probability component Gaussians (17.6 ± 2.9 ka; 20.9 ± 0.9 ka). This
412 distribution explains the larger number of samples required at both 1σ and 2σ relative to the
413 Arànsers left moraine. Ultimately, as the degree of overlap between component Gaussians
414 increases, more samples are required to isolate the highest probability component Gaussian
415 and eliminate PDE skew. Despite this, all landform ages could be reproduced with relatively
416 few samples at both 1σ ($n \leq 40$) and 2σ ($n \leq 26$). While these values exceed typical sample
417 size recommendations for TCN dating (Putkonen and Swanson, 2003), they are based upon
418 strict thresholds ($\geq 95\%$ of simulated landform ages within 1σ or 2σ of the full dataset
419 landform age) and should be utilised by researchers when pre-screening a larger population
420 of boulders prior to targeted TCN sampling.

421 **4. Discussion**

422 Efforts to minimise sampling bias of moraine TCN datasets may significantly improve the
423 utility of moraine chronologies in determining glacial history and the climatic drivers of
424 glacial cycles. However, while careful geomorphological assessment of individual boulders is
425 necessary to isolate those influenced by pre- or post-depositional processes, many criteria
426 for TCN sample selection have not been tested quantitatively. Of these, boulder location is
427 traditionally thought to be critical, as moraine crest boulders are prioritised due to
428 perceived stability (e.g. Gosse et al., 1995; Hallet and Putkonen, 1994), while those
429 deposited on ice-proximal or -distal slopes are typically rejected. This study is the first to
430 quantitatively assess this approach.

431 Based on ^{10}Be ($n = 10$) and Schmidt hammer sampling ($n = 635$) of ice-marginal moraines in
432 the Pyrenees, it is clear that the spatial distribution of SH-calibrated exposure ages is both
433 complex and site-specific. For many moraines, the distribution of “good” and “bad” boulders
434 is effectively random ($p > 0.05$), as assessed using global Moran’s I (Table 3), while in others,
435 clusters of “good” and “bad” boulders have clear geomorphological explanations. More
436 fundamentally, the likelihood of selecting a “good” boulder is comparable for moraine
437 crests, ice-proximal and -distal slopes (Fig. 7A). Although statistically significant spatial
438 clustering is evident for the Arànsér left and Soum d’Ech moraines ($p < 0.05$; Fig. 6), the
439 distribution of “good” boulder clusters is complex, with clusters distributed across moraine
440 crests and moraine slopes.

441 While there are no consistent spatial patterns at the inter-landform scale, the temporal
442 distribution of SH-calibrated exposure ages varies markedly between the studied landforms,
443 with a number of important observations. First, moraine sedimentology appears to place a
444 key control on post-depositional stability (Zreda et al., 1994; Putkonen and O’Neal, 2006),
445 as age distributions for matrix-rich moraines (e.g. Arànsér, Soum d’Ech) are strongly

446 negatively skewed (Fig. 6), with many boulders younger than the assigned age of the
447 landform. The frequency of “young” boulders for these moraines (Table 2) likely reflects the
448 influence of diffusive slope processes (Applegate et al., 2010), as the transfer of sediment to
449 the base of moraine slopes drives exhumation of entrained boulders (Porter and Swanson,
450 2008) and erosion of moraine crests (Schaller et al., 2009) and leads to increasingly subdued
451 moraine topography (Putkonen and O’Neal, 2006). The clearest signal of moraine
452 degradation is evident at the Arànsér left (IQR = 7.9 ka; Skew = -1.02) and Arànsér right
453 moraines (IQR = 6.9 ka; Skew = -1.13) and this trend may be partially explained by forest
454 growth and boulder toppling (Ivy-Ochs et al., 2007), as well as the effects of fluvial incision
455 (Fig. 6), while historic land use may also play a role (Pallàs et al., 2010).

456 In contrast, the boulder-rich, matrix-poor Outer Pleta Naua moraine stabilised rapidly after
457 glacial retreat, as evidenced by the distribution and clustering of both its SH-calibrated
458 exposure ages (IQR = 0.6 ka; Shapiro Wilk $W = 0.96$, $p = 0.07$) and the corresponding ^{10}Be
459 dataset (Pallàs et al., 2006). The sedimentology of the Outer Pleta Naua moraine is likely a
460 function of catchment size and glacier area, and the short transport distance from the
461 bedrock source area (Fig. 3; ≤ 300 m). In the absence of a supporting sediment matrix,
462 boulder-rich moraines stabilise quickly and appear less susceptible to subsequent erosion
463 (Ivy-Ochs et al., 2007; Pallàs et al., 2010). Finally, for moraines deposited by niche cirque
464 glaciers, reworking of glacial, periglacial or rockfall material appears more significant than
465 post-depositional modification, in line with previous studies (Heyman et al., 2011). In these
466 environments, the age of the oldest boulder may overestimate the “true” age of the
467 moraine (Putkonen and Swanson, 2003; Briner et al., 2005).

468 **Implications for TCN sampling of moraines**

469 The results described above have implications for future sampling approaches. First, while
470 “good” boulders are not more likely on moraine crests, we find there is no clear penalty to
471 moraine crest sampling, as initial differences between moraine crests and ice-proximal and -
472 distal slopes appear to be masked by continued moraine degradation. Thus, in the absence
473 of detailed geomorphological assessments of individual landforms, restricting sampling to
474 moraine crests is a viable strategy to minimise the likelihood of boulder instability, assuming
475 there are sufficient numbers of boulders to select from. This finding is unlikely to hold true
476 for recently deposited (< 1 ka) unconsolidated landforms (Putkonen and O’Neal, 2006),
477 whose over-steepened ice-proximal slopes have yet to stabilise (Briner et al., 2005; Dortch
478 et al., 2010).

479 Second, our results show that sampling boulders on ice-proximal and -distal slopes can be as
480 effective as sampling moraine crests (Fig. 7A). While boulder density is typically highest at
481 moraine crests (Putkonen et al., 2008), there is no guarantee that these boulders are the
482 best options for TCN dating. Moreover, if sample selection criteria are rigorously applied,
483 the number of suitable boulders available for dating could fall below a critical level. Without
484 robust statistical identification of outliers, this could lead to unclear results given the
485 ubiquity of post-depositional modification of moraines (Zech et al., 2005; Heyman et al.,
486 2011). One strategy which is rarely utilised is to select boulders for TCN dating from ice-
487 proximal and -distal slopes, but evidence from the studied moraines indicates that this is a
488 viable strategy, as the proportion of “good” boulders is comparable to moraine crests (Fig.
489 7A). For many moraines, the spatial distribution of “good” boulders is random, while
490 statistically significant clusters of “good” boulders are distributed across moraine crests and
491 moraine slopes (Fig. 6). These observations indicate that redefining selection criteria to
492 include the entire population of moraine boulders would have no clear negative effect and

493 could prove beneficial for moraines where ideal boulders are rare or are distributed away
494 from moraine crests.

495 Third, our data indicate that landform characteristics have a clear impact on the temporal
496 distribution of SH-calibrated exposure ages (Fig. 5; Putkonen and O’Neal, 2006; Ivy-Ochs et
497 al., 2007; Pallàs et al., 2010). Within this context, we suggest that landform stability should
498 be prioritised, as differences between landforms appear far greater than differences between
499 boulder groups on an individual landform (C vs. IS vs. OS). Differences are evident as a
500 function of moraine sedimentology (Zreda et al., 1994), with rapid stabilisation of matrix-
501 poor, boulder-rich moraines (e.g. Outer Pleta Naua; Pallàs et al., 2006; 2010; Ivy-Ochs et al.,
502 2007) but prolonged degradation of unconsolidated landforms (e.g. Arànsér; Putkonen and
503 O’Neal, 2006; Dortch et al., 2010). Although moraine sedimentology has explanatory power
504 for the studied moraines, the observed trends are unlikely to hold true in all settings due to
505 climatic and topographic controls on moraine stability (Barr and Lovell, 2014). Moreover,
506 restricting sampling to matrix-poor landforms could have unintended adverse effects, as
507 moraines may incorporate supraglacial rock avalanche debris and may primarily preserve a
508 non-climatic signal. Alternatively, sampling unconsolidated landforms does not guarantee
509 poor clustering (e.g. $\chi^2 > 1$), particularly in regions where moraine denudation is limited by
510 climate (Zech et al., 2005; Morgan et al., 2011; Balter et al., 2020) or where topographic
511 factors promote moraine stability (Barr and Lovell, 2014). Finally, restricting sampling to
512 landforms with specific characteristics is often not viable, as key glacial chronological
513 markers may be represented by only a small number of landforms.

514 Within this context, we suggest that landform selection is critical, and care should be taken
515 to select methods which are appropriate for its assumed age and stability and to collect a
516 sufficient number of samples to enable robust outlier identification (Putkonen and Swanson,

517 2003). However, it is often challenging to assess landform stability based on
518 geomorphological evidence alone. Our approach, in light of strong regional evidence for an
519 inverse correlation between SH *R*-values and exposure ages for granitic surfaces (Tomkins
520 et al., 2018a; 2018b), indicates that preliminary SH sampling could be a useful method to
521 assess landform stability, to identify boulders affected by post-depositional processes, and to
522 prioritise individual boulders for analysis based on *R*-value clustering (Tylmann et al., 2018).

523 Based on the sensitivity approach described in Section 2.6, the number of SH samples
524 required scales with the complexity of the underlying distribution (Fig. 7B), from those
525 which are approximately normal to those which feature overlapping component Gaussian
526 distributions (Fig. 5) or multi-directional skew (i.e. pre- and post-depositional skew).
527 However, given that it is not possible to ascertain the underlying distribution a priori, a
528 relatively large sample size is ultimately required. For most landforms, sampling a minimum
529 of ~30 boulders would be a reasonable approach to estimate a depositional age within 2σ (n
530 ≥ 23), but more would be required ($n \geq 40$) to improve precision to 1σ for complex
531 datasets or if Schmidt hammer *R*-values were being used as a basis for cosmogenic nuclide
532 sample selection (Tylmann et al., 2018). Collecting a minimum of 30 – 40 samples is
533 necessary to ensure a full understanding of the underlying age distribution, even for complex
534 datasets. Based on this preliminary sampling, statistical approaches could be used to isolate
535 component Gaussian distributions (Dortch et al., 2013; 2021) and to identify individual
536 boulders which are consistent with the age of the landform and to reject those which are
537 “young” or “old” (Heyman et al., 2011).

538 Finally, it is important to note that the effectiveness of this approach may vary as a function
539 of lithology and climate (McCarroll, 1989), while the underlying measurements are sensitive
540 to factors which have only a minor effect on cosmogenic nuclide concentrations (e.g. surface

541 discontinuities, Williams and Robinson, 1983; lichen coverage, Matthews and Owen, 2008).
542 However, when these limitations are accounted for, Schmidt hammer *R*-values can be used
543 as a proxy for surface exposure age (Fig. 4). Given the ubiquity of geologic scatter (e.g.
544 exhumation, erosion, shielding), incorporating time- and cost-efficient preliminary SH
545 sampling as an additional tool for TCN sample selection could ultimately improve the
546 chronological utility of the moraine record and enable a deeper understanding of the
547 climatic drivers of glacial cycles.

548 **Conclusions**

549 Based on ^{10}Be and Schmidt hammer sampling of ice-marginal moraines in the Pyrenees, this
550 study provided the first quantitative analysis of the relative utility of moraine crest and
551 moraine slope sampling for terrestrial cosmogenic nuclide dating. Using spatial analysis of
552 SH-calibrated exposure ages, we show that there is no clear penalty to moraine slope
553 sampling. However, contrary to current sampling approaches, which typically prioritise
554 moraine crest boulders due to perceived stability, we show that the proportion of “good”
555 boulders is comparable between moraine crests and ice-proximal and -distal slopes, while
556 for many moraines, the spatial distribution of “good” boulders is effectively random.
557 Crucially, however, differences between landforms appear more significant than differences
558 at the intra-landform scale; a result which indicates that the stability of the landform can
559 have a far greater impact on the distribution of boulder exposure ages than the
560 characteristics and depositional context of individual boulders. In this study, moraine
561 sedimentology likely accounts for the observed differences between landforms, with rapid
562 stabilisation of matrix-poor, boulder-rich moraines and prolonged degradation for
563 unconsolidated landforms. Although these trends are unlikely to be universally applicable
564 given climatic and topographic controls on moraine stability, our data indicate that

565 preliminary SH sampling is a valuable tool to assess landform stability and to prioritise
566 individual boulders for further analysis.

567 **Acknowledgements**

568 MT was funded by a University of Manchester President's Doctoral Scholar Award. The
569 fieldwork for this paper was supported by a British Society for Geomorphology
570 Postgraduate Research grant awarded to MT. ^{10}Be analysis was performed at the ASTER
571 AMS national facility (CEREGE), which is supported by the CNRS/INSU, by the ANR,
572 through the "projets thématiques d'excellence" programme for the "Equipements
573 d'excellence" ASTER-CEREGE action, and by the Institut de Recherche pour le
574 Développement (IRD). MT, JD, PH and RP designed the project, with refinements from IB
575 and CD. MT, JA and AS conducted Schmidt hammer sampling. ^{10}Be sampling and analysis
576 was undertaken by RP, AR, DB, VR, VJ, LRR and RC. MT and JH conducted spatial analysis.
577 MT, JH and TB improved error propagation. All authors contributed to the manuscript. We
578 would like to thank Professor W. Amidon for his constructive review. We thank Dr. G.
579 Evatt and Dr. A. Smedley at the University of Manchester for their comments, D. Tomkins
580 and Dr. B. van Bodegraven for fieldwork support, and the contributors to the open-source
581 libraries PySAL and GeoPandas.

582 **Word Count: 6500**

583

584

Table 1. Summary data for terrestrial cosmogenic exposure ages from the sampled moraines^a

Moraine	Name	Isotope	Latitude (°)	Longitude (°)	Elevation (m)	Age (ka)	Internal ± (ka)	External ± (ka)	SH R ± SEM ^b	
Outer Pleta Naua ^c	OPN01	¹⁰ Be	42.6365	0.7399	2217	13.2	1.3	1.6	-	
	OPN02	¹⁰ Be	42.6365	0.7406	2197	13.0	1.7	2.0	51.68 ± 0.5	
	OPN03	¹⁰ Be	42.6365	0.7409	2195	12.6	1.2	1.5	-	
Arànsers (Right) ^d	SAL-01	¹⁰ Be	42.4283	1.6300	2000	17.6	0.6	1.5	47.57 ± 0.83	
	SAL-02	¹⁰ Be	42.4273	1.6321	1983	19.2	0.6	1.5	45.07 ± 0.84	
	SAL-03	¹⁰ Be	42.4270	1.6326	1975	21.1	0.6	1.7	44.07 ± 0.82	
	SAL-04	¹⁰ Be	42.4254	1.6358	1933	18.0	0.6	1.5	47.57 ± 0.84	
	SAL-05	¹⁰ Be	42.4240	1.6389	1912	17.0	0.9	1.6	48.9 ± 0.77	
	SAL-06	¹⁰ Be	42.4237	1.6395	1908	19.2	0.6	1.5	44.53 ± 0.74	
	SAL-07	¹⁰ Be	42.4229	1.6415	1896	16.7	0.5	1.4	47.43 ± 0.96	
	SAL-08	¹⁰ Be	42.4223	1.6447	1863	17.1	0.6	1.4	47.7 ± 0.9	
	SAL-09	¹⁰ Be	42.4215	1.6481	1820	20.7	0.9	1.7	44.77 ± 0.8	
	SAL-10	¹⁰ Be	42.4213	1.6489	1808	22.4	0.7	1.8	43.03 ± 0.95	
	PIR-11-13	³⁶ Cl	42.4213	1.6495	1809	18.2	1.6	2.1	-	
	PIR-11-14	³⁶ Cl	42.4209	1.6499	1805	17.3	1.7	2.2	47.6 ± 0.83	
	Soum d'Eche ^e	ECH01	¹⁰ Be	43.0863	-0.0870	776	19.7	3.2	3.6	42.43 ± 0.98
		ECH02	¹⁰ Be	43.0858	-0.0880	778	59.0	43.2 ^f	43.0	-
ECH03		¹⁰ Be	43.0862	-0.0873	779	17.2	3.3	3.5	38.86 ± 1.11	
ECH04		¹⁰ Be	43.0865	-0.0867	781	16.8	3.0	3.3	38.77 ± 1.05	

^a Full sample information used for exposure age calculation is provided in the Supplementary Information or is available on GitHub:

<https://github.com/matt-tomkins/moraine-crest-or-slope>, ^b Mean of 30 SH R-values ± the Standard Error of the Mean, ^c OPN samples from Pallàs et al. (2006), ^d PIR samples from Palacios et al. (2015), ^e ECH samples from Rodés (2008), ^f Measurement error, see Rodés (2008).

Table 2. Age statistics for the sampled moraines

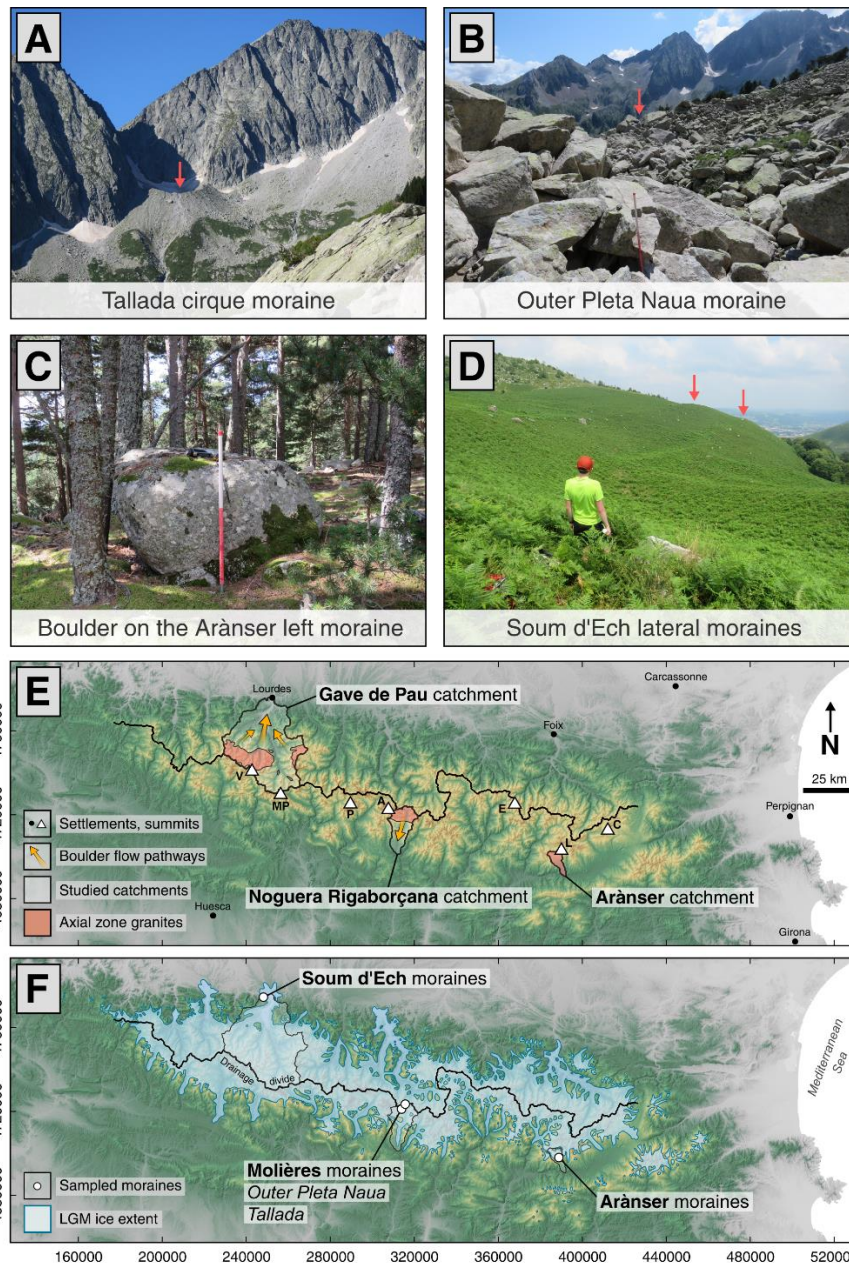
Moraine	Group	Method ^a	Bandwidth ^b	Model fit ^c	Age (ka) ^d	IQR ^e	Skew	Normality ^f	Young (%) ^g	Good (%) ^g	Old (%) ^g
Tallada	-	STD / IQR	0.3731	0.9985	3.2 ± 0.7	1.2 ka	0.34	0.44	6	80	14
Outer Pleta Naua	-	Mean	2.016	1	12.5 ± 0.4 ^h	0.6 ka	-0.24	0.07	0	100	0
Arànsér	Left	MAD	0.7003	0.9978	23.3 ± 1.1 ⁱ	7.9 ka	-1.02	< 0.01	44	56	0
	Right	MAD	0.6796	0.9991	22.3 ± 0.9	6.9 ka	-1.13	< 0.01	51	49	0
Soum d'Ech	Outer	STD / IQR	1.0734	0.998	26.2 ± 2.5	3.5 ka	-1.49	< 0.01	-	-	-
	Inner	STD / IQR	1.1661	0.9996	26.1 ± 1.7	3.5 ka	-1.05	< 0.01	-	-	-
	Combined	STD / IQR	0.9877	0.9989	27.3 ± 1.8	3.6 ka	-1.49	< 0.01	24	76	0

^{a,b} Method used for kernel density estimation (see Dortch *et al.*, 2021) and its associated numeric bandwidth, ^c All model *p* values < 0.01, ^d Reported uncertainty (\pm) is the 1 σ bounds (68%) of the highest probability component Gaussian, unless stated otherwise, ^e Interquartile range, ^f Shapiro-Wilk test for normality *p* values, ^g Based on the landform age $\pm 2\sigma$, ^h Arithmetic mean of 60 samples \pm total uncertainty, ⁱ Calculation based on a reduced dataset of 274 samples. Sample ARL-192 (1.97 \pm 2.06 ka) is more than three standard deviations from the mean of the remaining samples and was removed for program stability.

Table 3. Spatial statistics for the sampled moraines

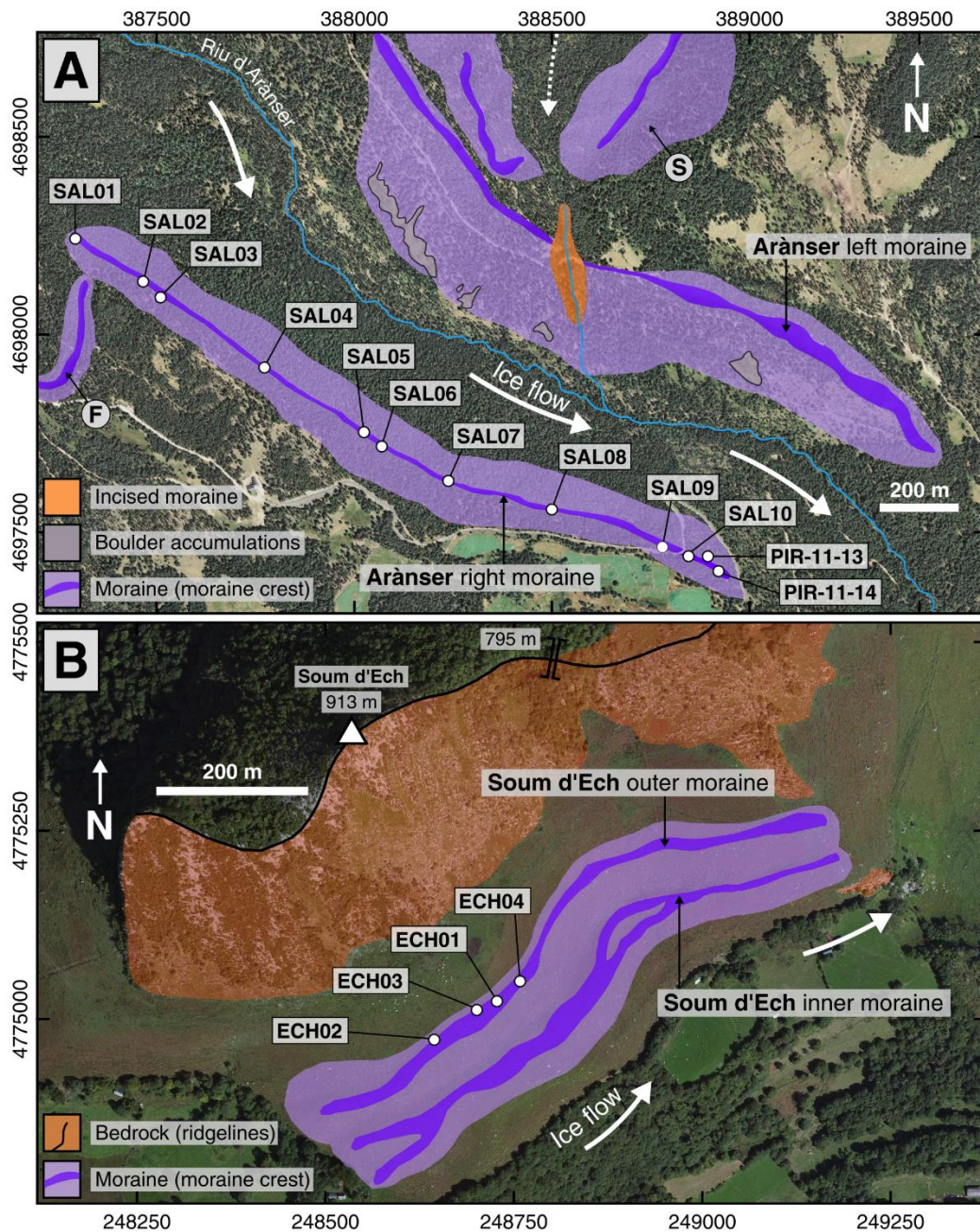
Moraine	Type	Number of samples				Global Morans <i>I</i>			“Good” boulder (%)		
		Total	IS ^a	C ^a	OS ^a	Distance threshold (m) ^b	<i>I</i>	Simulated <i>p</i> value ^c	IS ^a	C ^a	OS ^a
Tallada	Terminal	70	16	29	25	21.6	0.0980	0.0719	80	79	81
Outer Pleta Naua	Terminal	60	20	20	20	23.9	NA ^d	NA ^d	100	100	100
Arànsér (Left)	Latero-frontal	275	199	51	25	59.5	0.0915	0.0064	53	57	76
Arànsér (Right)	Latero-frontal	130	57	33	40	66.3	0.0651	0.1194	63	36	40
Soum d’Ech	Laterals	100	37	50	13	51.1	0.1519	0.0106	76	72	81

^a Inner ice-proximal slope (IS), moraine crest (C) and outer ice-distal slope (OS), ^b Defined as the minimum distance required to ensure that each boulder has at least two neighbours, ^c *p* values > 0.05 support no statistically significant spatial clustering. *p* values ≤ 0.05 are consistent with a non-random distribution and spatial clustering of the input data, ^d Spatial autocorrelation was not possible for the Outer Pleta Naua moraine as all boulders were classed as "good" based on the 2σ threshold.



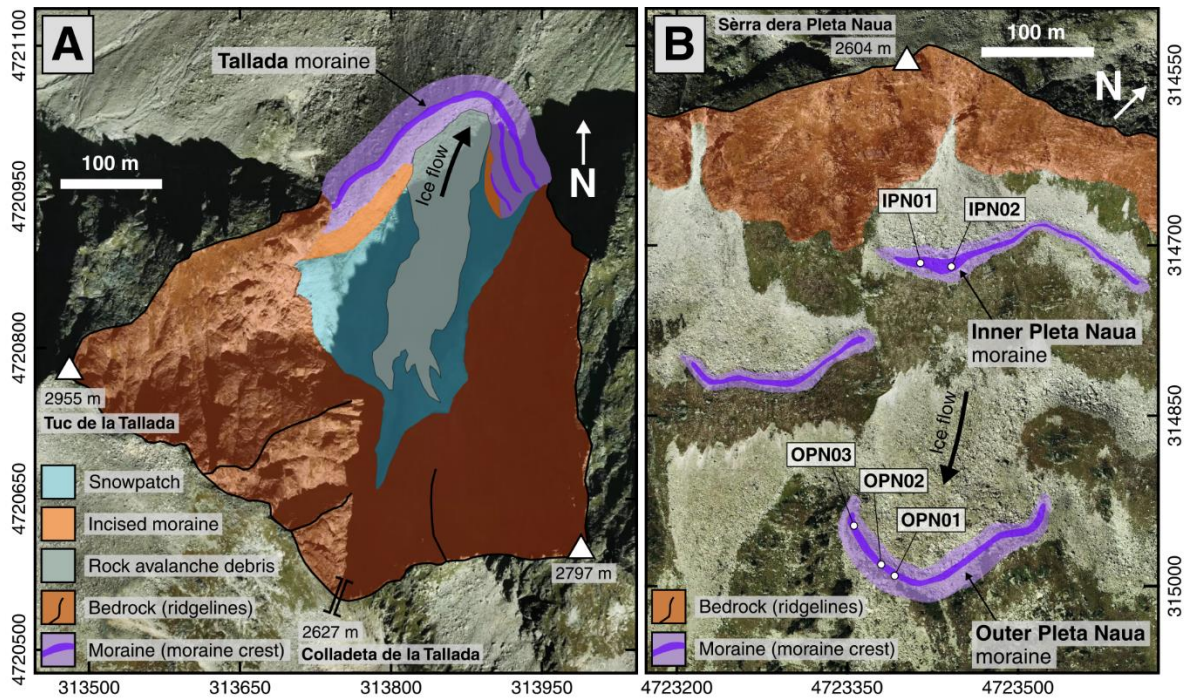
588

589 **Figure 1.** Site photographs of the (A) Tallada, (B) Outer Pleta Naua, (C) Arànsers and (D) Soum
 590 d'Ech moraines (denoted by red arrows). (E-F) Topographic maps of the Pyrenees (ASTER GDEM
 591 V3, WGS 84 UTM 31N), showing the locations of the studied catchments and selected moraines and
 592 the distribution of Axial Zone granites within those catchments. The latter was derived from a
 593 1:400,000 geological map produced by the IGME (Spain) and the BRGM (France). Also shown are the
 594 locations of major summits (**A**neto, **C**arlit, **E**stats, **P**lana de **L**les, **M**onte **P**erdido, **P**osets,
 595 **V**ignemale) and the extent of glaciers during the global Last Glacial Maximum (LGM; Calvet et al.,
 596 2011).



597

598 **Figure 2.** Geomorphological maps for the (A) Arànsers and (B) Soum d'Ech moraines (WGS 84
 599 UTM 31N). These moraines likely correspond to the maximum ice extent (MIE) during the
 600 Würmian glacial stage (11.7 - 11.0 ka; Calvet et al., 2011). Locations and sample names for TCN
 601 dated boulders are shown (white circles; Rodés, 2008; Palacios et al., 2015). In (A), the locations of
 602 the proximal Fornell (F) and Setut (S) moraines are highlighted. These moraines are stratigraphically
 603 distinct from the sampled Arànsers moraines but are currently undated. The margins of Arànsers
 604 glacier can be traced further up valley but sampling was focused on the illustrated moraine area (light
 605 purple shading) in which the moraine margins are easily delineated (≤ 2 km from glacier terminus).



606

607 **Figure 3.** Geomorphological maps for the (A) Tallada and (B) Outer Pleta Naua moraines in the Val

608 de Molières catchment of the Noguera Rigaborçana (WGS 84 UTM 3 IN). Locations and sample

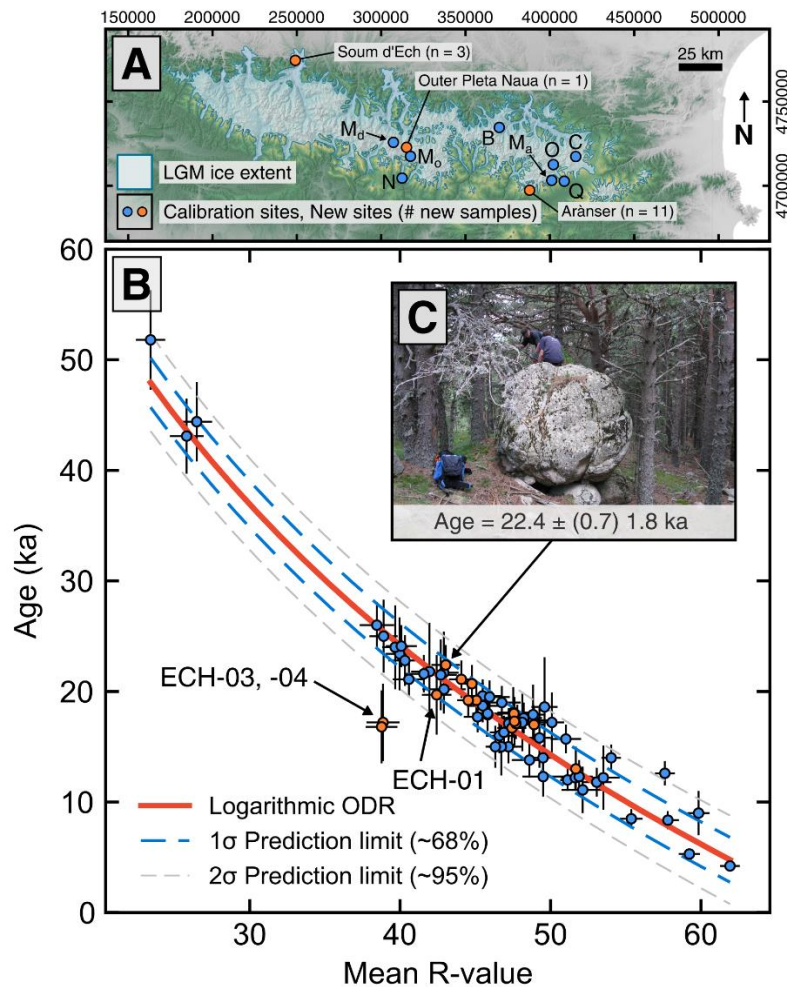
609 names for TCN dated boulders are shown (white circles; Pallàs et al., 2006). The Inner Pleta Naua

610 moraine was also investigated by Pallàs et al., (2006) and returned recalculated ^{10}Be ages of 6.3 ± 0.9

611 ka (IPN01) and 16.0 ± 2.5 ka (IPN02). Given the stratigraphic position of this deposit and limiting

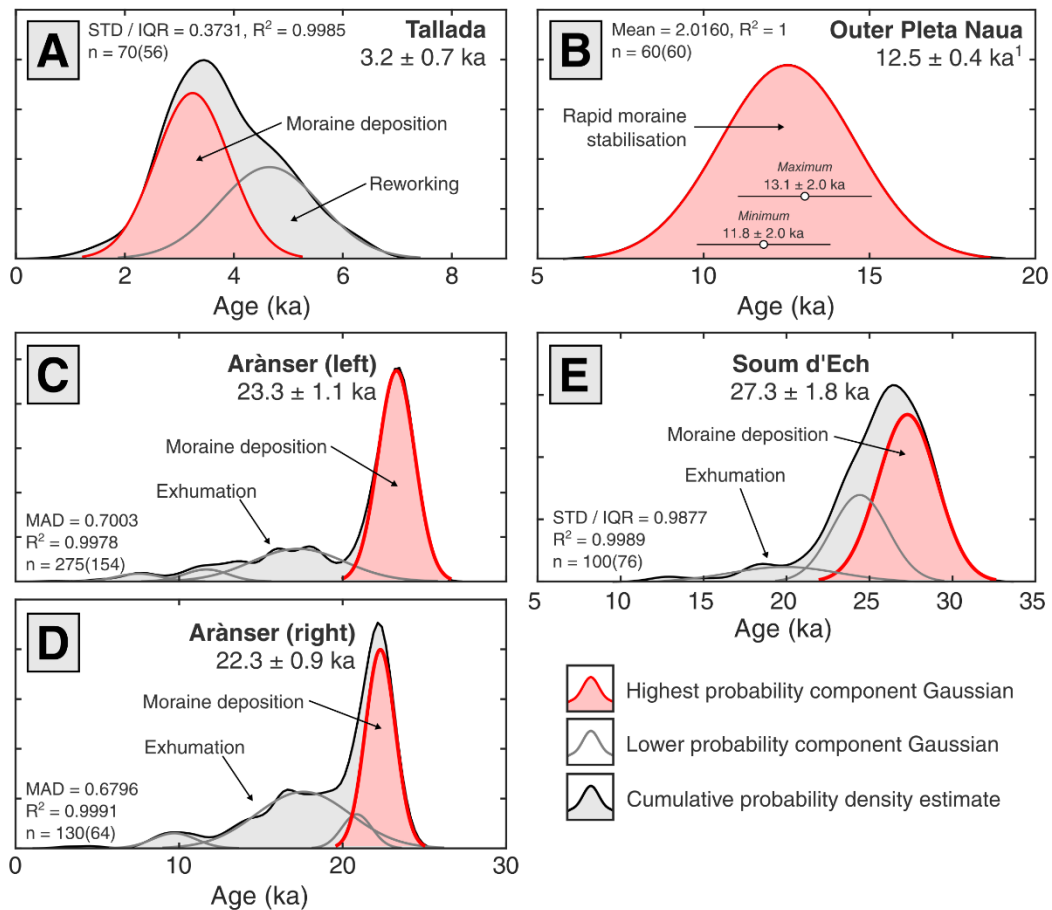
612 ages from the Outer Pleta Naua and Molières moraines (MUL01 = 14.9 ± 2.6 ka, MUL03 = $14.9 \pm$

613 1.9 ka; Pallàs et al., 2006), it appears likely that IPN02 is affected by inheritance.



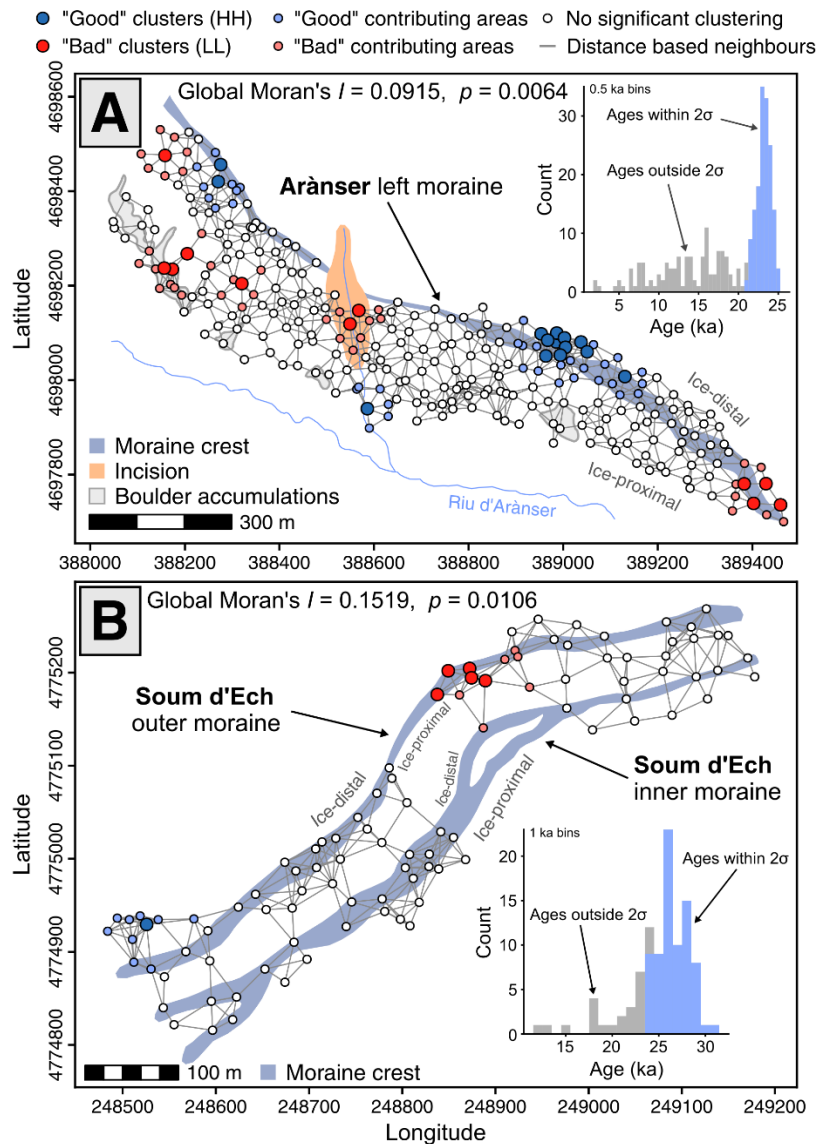
614

615 **Figure 4.** (A) Location of exposure age calibration sites (blue points) in the Bassies (B, $n = 6$), Carlit
 616 (C, $n = 3$), Noguera Rigaborçana (N, $n = 4$), Maladeta (M_a , $n = 9$), Malniu (M_n , $n = 21$), Molières (M_o , n
 617 = 2), Orri (O, $n = 3$) and Querol catchments (Q, $n = 6$). Underlying topography is ASTER GDEM V3
 618 (WGS 84 UTM 31N). Also shown are the locations of sampled moraines (orange points; see Fig. 1F)
 619 and the maximum ice extent (MIE) during the global Last Glacial Maximum (LGM; Calvet et al., 2011).
 620 (B) Monte Carlo-derived orthogonal distance regression (ODR) between 54 ^{10}Be exposure ages (blue
 621 points \pm external age uncertainty) and their corresponding SH R -values (mean of 30 R -values \pm
 622 Standard Error of the Mean; Tomkins et al., 2018b), plus 1σ (blue dashed lines) and 2σ prediction
 623 limits (grey dashed lines). Independent TCN samples (^{10}Be , ^{36}Cl) from the studied moraines ($n = 15$)
 624 are shown as orange points. Inherited outliers from the original calibration dataset ($n = 2$; Tomkins et
 625 al., 2018b) are not shown for clarity. (C) Example of a ^{10}Be dated boulder from the Arànsers right
 626 moraine (SAL-10).



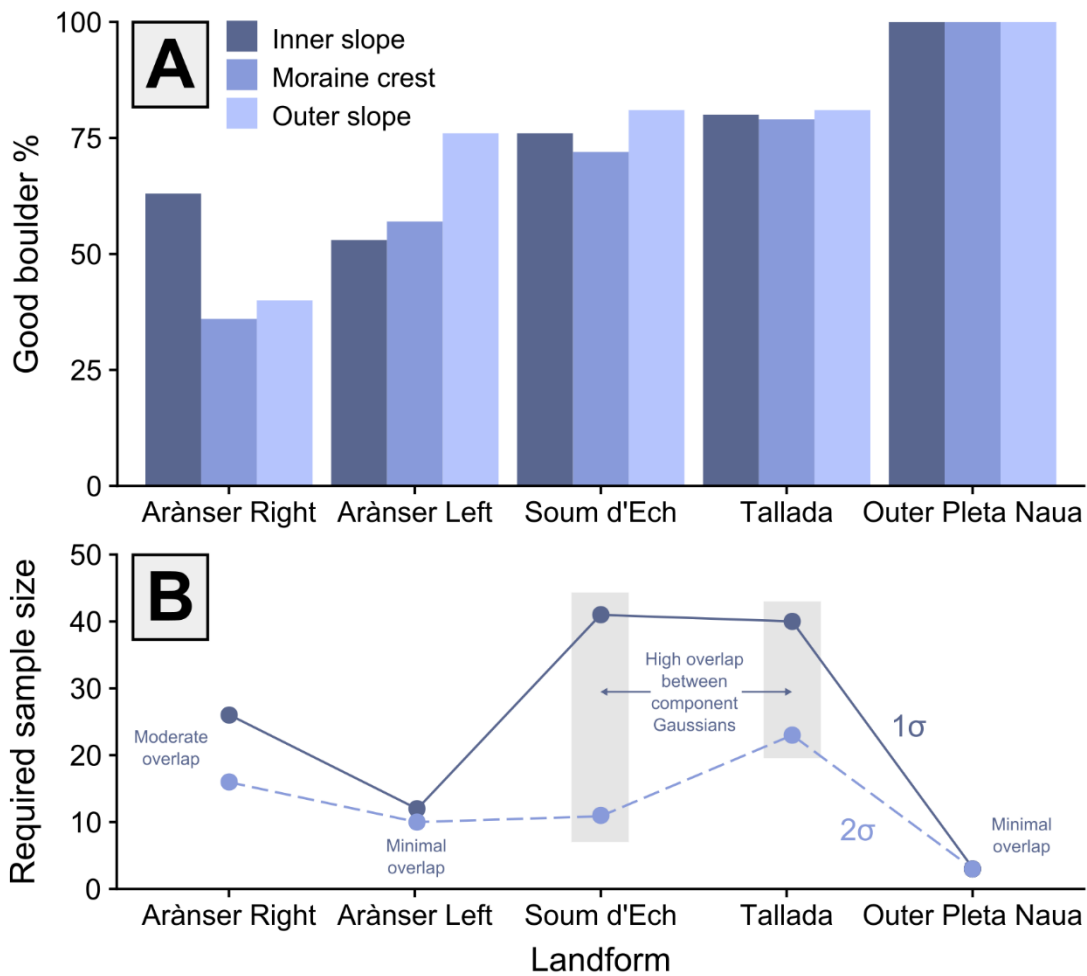
627

628 **Figure 5.** Gaussian decomposition of SH-calibrated boulder exposure ages for the Tallada (A),
 629 Outer Pleta Naua (B), Arànsér (C-D) and Soum d'Ech moraines (E). Following P-CAAT guidelines
 630 (Dortch et al., 2013; 2021), we selected the highest probability component Gaussian (red shading) to
 631 represent the age of the landform as all are \leq LGM. The summed probability density estimate (PDE)
 632 and lower probability component Gaussians are denoted by black and grey distributions,
 633 respectively. For each moraine, we include the bandwidth estimator used and its associated numeric
 634 bandwidth, the P-CAAT model fit (R^2), the total number of SH-calibrated exposure ages (n) and in
 635 brackets, the number of ages which are enclosed by the selected component Gaussian distribution at
 636 2σ . Based on this approach, selected component Gaussians are interpreted to reflect the timing of
 637 moraine deposition or initial stabilisation. In contrast, younger component Gaussians may reflect
 638 post-depositional processes (e.g. moraine degradation, boulder exhumation or instability) while
 639 older component Gaussians likely incorporate pre-depositional processes (e.g. reworking of glacial
 640 deposits).



641

642 **Figure 6.** Results of local Moran's I spatial autocorrelation for the Arànsers left (A) and Soum d'Ech
 643 moraines (B). Points denote the location of sampled boulders, with neighbouring boulders linked by
 644 grey lines. Neighbours are calculated based on a fixed distance, defined as the minimum distance
 645 required to ensure that each boulder has at least two neighbours, and were analysed using inverse
 646 distance weighted (IDW). Points are coloured based on the results of local Moran's I , with regions of
 647 no statistically significant spatial clustering shown as white, while clusters of "good" (HH) and "bad"
 648 boulders (LL) and their contributing neighbours are shown in blue and red, respectively. Outlier
 649 points (HL and LH) are not shown for clarity. A histogram illustrating the distribution of calibrated
 650 boulder exposure ages is included for each moraine, coloured by the "good" (blue) and "bad"
 651 components (grey).



652

653 **Figure 7.** The likelihood of sampling a “good” boulder (%; within 2σ of the landform age) for each
 654 of the studied moraines (A), subset by boulder position (inner ice-proximal slope, moraine crest,
 655 outer ice-distal slope). Sensitivity results are shown for each moraine (B), illustrating the number of
 656 samples required to reproduce the associated landform age within 1σ and 2σ thresholds.

657

658

659

660

661

662 **References**

- 663 Applegate, P.J., Urban, N.M., Keller, K., Lowell, T.V., Laabs, B.J.C., Kelly, M.A., Alley, R.B., 2012. Improved
664 moraine age interpretations through explicit matching of geomorphic process models to cosmogenic
665 nuclide measurements from single landforms. *Quaternary Research* 77, 293–304.
666 <https://doi.org/10.1016/j.yqres.2011.12.002>
- 667 Applegate, P.J., Urban, N.M., Laabs, B.J.C., Keller, K., Alley, R.B., 2010. Modeling the statistical distributions of
668 cosmogenic exposure dates from moraines. *Geoscientific Model Development* 3, 293–307.
669 <https://doi.org/10.5194/gmd-3-293-2010>
- 670 Balter, A., Bromley, G., Balco, G., Thomas, H., Jackson, M.S., 2020. A 14.5-million-year record of East Antarctic
671 Ice Sheet fluctuations from the central Transantarctic Mountains, constrained with cosmogenic ^3He , ^{10}Be ,
672 ^{21}Ne , and ^{26}Al . *The Cryosphere Discussions* 1–41. <https://doi.org/10.5194/tc-2020-57>
- 673 Barr, I.D., Lovell, H., 2014. A review of topographic controls on moraine distribution. *Geomorphology* 226,
674 44–64. <https://doi.org/10.1016/j.geomorph.2014.07.030>
- 675 Boggs, Paul T., Rogers, J.E., 1990. Orthogonal distance regression, in: “Statistical Analysis of Measurement
676 Error Models and Applications: Proceedings of the AMS-IMS-SIAM Joint Summer Research Conference
677 Held June 10-16, 1989,” Presented at the Contemporary Mathematics, p. 186.
678 <https://doi.org/10.6028/nist.ir.89-4197>
- 679 Borchers, B., Marrero, S., Balco, G., Caffee, M., Goehring, B., Lifton, N., Nishiizumi, K., Phillips, F., Schaefer, J.,
680 Stone, J., 2016. Geological calibration of spallation production rates in the CRONUS-Earth project.
681 *Quaternary Geochronology* 31, 188–198. <https://doi.org/10.1016/j.quageo.2015.01.009>
- 682 Briner, J.P., Kaufman, D.S., Manley, W.F., Finkel, R.C., Caffee, M.W., 2005. Cosmogenic exposure dating of late
683 Pleistocene moraine stabilization in Alaska. *GSA Bulletin* 117, 1108–1120.
684 <https://doi.org/10.1130/B25649.1>
- 685 Calvet, M., Delmas, M., Gunnell, Y., Braucher, R., Bourlès, D., 2011. Chapter 11 - Recent Advances in Research
686 on Quaternary Glaciations in the Pyrenees, in: Ehlers, J., Gibbard, P.L., Hughes, P.D. (Eds.), *Developments
687 in Quaternary Sciences, Quaternary Glaciations - Extent and Chronology*. Elsevier, 127–139.
688 <https://doi.org/10.1016/B978-0-444-53447-7.00011-8>

689 Chevalier, M.-L., Replumaz, A., 2019. Deciphering old moraine age distributions in SE Tibet showing bimodal
690 climatic signal for glaciations: Marine Isotope Stages 2 and 6. *Earth and Planetary Science Letters* 507, 105–
691 118. <https://doi.org/10.1016/j.epsl.2018.11.033>

692 Darmody, R.G., Thorn, C.E., Allen, C.E., 2005. Chemical weathering and boulder mantles, Kärkevagge, Swedish
693 Lapland. *Geomorphology, Weathering and landscape evolution* 67, 159–170.
694 <https://doi.org/10.1016/j.geomorph.2004.07.011>

695 Darvill, C.M., Bentley, M.J., Stokes, C.R., 2015. Geomorphology and weathering characteristics of erratic
696 boulder trains on Tierra del Fuego, southernmost South America: Implications for dating of glacial
697 deposits. *Geomorphology* 228, 382–397. <https://doi.org/10.1016/j.geomorph.2014.09.017>

698 Dortch, J.M., Owen, L.A., Caffee, M.W., Li, D., Lowell, T.V., 2010. Beryllium-10 surface exposure dating of
699 glacial successions in the Central Alaska Range. *Journal of Quaternary Science* 25, 1259–1269.
700 <https://doi.org/10.1002/jqs.1406>

701 Dortch, J.M., Owen, L.A., Caffee, M.W., 2013. Timing and climatic drivers for glaciation across semi-arid
702 western Himalayan–Tibetan orogen. *Quaternary Science Reviews* 78, 188–208.
703 <https://doi.org/10.1016/j.quascirev.2013.07.025>

704 Dortch, J.M., Tomkins, M.D., Saha, S., Murari, M.K., Schoenbohm, L.M., Curl, D., 2021. Probabilistic
705 Cosmogenic Age Analysis Tool (P-CAAT), a tool for the ages. Manuscript in preparation.

706 Ehlmann, B.L., Viles, H.A., Bourke, M.C., 2008. Quantitative morphologic analysis of boulder shape and surface
707 texture to infer environmental history: A case study of rock breakdown at the Ephrata Fan, Channeled
708 Scabland, Washington. *Journal of Geophysical Research: Earth Surface* 113.
709 <https://doi.org/10.1029/2007JF000872>

710 Gosse, J.C., Evenson, E.B., Klein, J., Lawn, B., Middleton, R., 1995. Precise cosmogenic ¹⁰Be measurements in
711 western North America: Support for a global Younger Dryas cooling event. *Geology* 23, 877–880.
712 [https://doi.org/10.1130/0091-7613\(1995\)023<0877:PCBMIW>2.3.CO;2](https://doi.org/10.1130/0091-7613(1995)023<0877:PCBMIW>2.3.CO;2)

713 Hallet, B., Putkonen, J., 1994. Surface Dating of Dynamic Landforms: Young Boulders on Aging Moraines.
714 *Science* 265, 937–940. <https://doi.org/10.1126/science.265.5174.937>

715 Heyman, J., Applegate, P.J., Blomdin, R., Gribenski, N., Harbor, J.M., Stroeven, A.P., 2016. Boulder height –
716 exposure age relationships from a global glacial ¹⁰Be compilation. *Quaternary Geochronology* 34, 1–11.
717 <https://doi.org/10.1016/j.quageo.2016.03.002>

718 Heyman, J., Stroeven, A.P., Harbor, J.M., Caffee, M.W., 2011. Too young or too old: Evaluating cosmogenic
719 exposure dating based on an analysis of compiled boulder exposure ages. *Earth and Planetary Science*
720 *Letters* 302, 71–80. <https://doi.org/10.1016/j.epsl.2010.11.040>

721 Ivy-Ochs, S., Kerschner, H., Schlüchter, C., 2007. Cosmogenic nuclides and the dating of Lateglacial and Early
722 Holocene glacier variations: The Alpine perspective. *Quaternary International, From the Swiss Alps to the*
723 *Crimean Mountains - Alpine Quaternary stratigraphy in a European context* 164–165, 53–63.
724 <https://doi.org/10.1016/j.quaint.2006.12.008>

725 Lal, D., 1991. Cosmic ray labeling of erosion surfaces: in situ nuclide production rates and erosion models.
726 *Earth and Planetary Science Letters* 104, 424–439. [https://doi.org/10.1016/0012-821X\(91\)90220-C](https://doi.org/10.1016/0012-821X(91)90220-C)

727 Marrero, S.M., Hein, A.S., Naylor, M., Attal, M., Shanks, R., Winter, K., Woodward, J., Dunning, S., Westoby,
728 M., Sugden, D., 2018. Controls on subaerial erosion rates in Antarctica. *Earth and Planetary Science*
729 *Letters* 501, 56–66. <https://doi.org/10.1016/j.epsl.2018.08.018>

730 Marrero, S.M., Phillips, F.M., Borchers, B., Lifton, N., Aumer, R., Balco, G., 2016. Cosmogenic nuclide
731 systematics and the CRONUScal program. *Quaternary Geochronology* 31, 160–187.
732 <https://doi.org/10.1016/j.quageo.2015.09.005>

733 Matthews, J.A., Owen, G., 2008. Endolithic lichens, rapid biological weathering and schmidt hammer r-values
734 on recently exposed rock surfaces: storbreen glacier foreland, jotunheimen, norway. *Geografiska Annaler:*
735 *Series A, Physical Geography* 90, 287–297. <https://doi.org/10.1111/j.1468-0459.2008.00346.x>

736 McCarroll, D., 1989. Potential and Limitations of the Schmidt Hammer for Relative-Age Dating: Field Tests on
737 Neoglacial Moraines, Jotunheimen, Southern Norway. *Arctic and Alpine Research* 21, 268–275.
738 <https://doi.org/10.2307/1551565>

739 Morgan, D.J., Putkonen, J., Balco, G., Stone, J., 2011. Degradation of glacial deposits quantified with cosmogenic
740 nuclides, Quartermain Mountains, Antarctica. *Earth Surface Processes and Landforms* 36, 217–228.
741 <https://doi.org/10.1002/esp.2039>

742 Niedzielski, T., Migoń, P., Placek, A., 2009. A minimum sample size required from Schmidt hammer
743 measurements. *Earth Surface Processes and Landforms* 34, 1713–1725. <https://doi.org/10.1002/esp.1851>

744 Palacios, D., Gómez-Ortiz, A., Andrés, N., Vázquez-Selem, L., Salvador-Franch, F., Oliva, M., 2015. Maximum
745 extent of Late Pleistocene glaciers and last deglaciation of La Cerdanya mountains, Southeastern Pyrenees.
746 *Geomorphology* 231, 116–129. <https://doi.org/10.1016/j.geomorph.2014.10.037>

747 Pallàs, R., Rodés, Á., Braucher, R., Bourlès, D., Delmas, M., Calvet, M., Gunnell, Y., 2010. Small, isolated glacial
748 catchments as priority targets for cosmogenic surface exposure dating of Pleistocene climate fluctuations,
749 southeastern Pyrenees. *Geology* 38, 891–894. <https://doi.org/10.1130/G31164.1>

750 Pallàs, R., Rodés, Á., Braucher, R., Carcaillet, J., Ortuño, M., Bordonau, J., Bourlès, D., Vilaplana, J.M., Masana,
751 E., Santanach, P., 2006. Late Pleistocene and Holocene glaciation in the Pyrenees: a critical review and new
752 evidence from ¹⁰Be exposure ages, south-central Pyrenees. *Quaternary Science Reviews* 25, 2937–2963.
753 <https://doi.org/10.1016/j.quascirev.2006.04.004>

754 Portenga, E.W., Bierman, P.R., 2011. Understanding Earth's eroding surface with ¹⁰Be. *GSAT* 21, 4–10.
755 <https://doi.org/10.1130/G111A.1>

756 Porter, S.C., Swanson, T.W., 2008. ³⁶Cl dating of the classic Pleistocene glacial record in the northeastern
757 Cascade Range, Washington. *Am J Sci* 308, 130–166. <https://doi.org/10.2475/02.2008.02>

758 Putkonen, J., Connolly, J., Orloff, T., 2008. Landscape evolution degrades the geologic signature of past
759 glaciations. *Geomorphology, Glacial Landscape Evolution - Implications for Glacial Processes, Patterns and*
760 *Reconstructions* 97, 208–217. <https://doi.org/10.1016/j.geomorph.2007.02.043>

761 Putkonen, J., O'Neal, M., 2006. Degradation of unconsolidated Quaternary landforms in the western North
762 America. *Geomorphology, Quaternary landscape change and modern process in western North America*
763 75, 408–419. <https://doi.org/10.1016/j.geomorph.2005.07.024>

764 Putkonen, J., Swanson, T., 2003. Accuracy of cosmogenic ages for moraines. *Quaternary Research* 59, 255–
765 261. [https://doi.org/10.1016/S0033-5894\(03\)00006-1](https://doi.org/10.1016/S0033-5894(03)00006-1)

766 Reille, M., Andrieu, V., 1995. The late Pleistocene and Holocene in the Lourdes Basin, Western Pyrénées,
767 France: new pollen analytical and chronological data. *Veget Hist Archaeobot* 4, 1–21.
768 <https://doi.org/10.1007/BF00198611>

769 Reimer, P.J., Bard, E., Bayliss, A., Beck, J.W., Blackwell, P.G., Ramsey, C.B., Buck, C.E., Cheng, H., Edwards, R.L.,
770 Friedrich, M., Grootes, P.M., Guilderson, T.P., Hafliðason, H., Hajdas, I., Hatté, C., Heaton, T.J., Hoffmann,
771 D.L., Hogg, A.G., Hughen, K.A., Kaiser, K.F., Kromer, B., Manning, S.W., Niu, M., Reimer, R.W., Richards,
772 D.A., Scott, E.M., Southon, J.R., Staff, R.A., Turney, C.S.M., Plicht, J. van der, 2013. IntCal13 and Marine13
773 Radiocarbon Age Calibration Curves 0–50,000 Years cal BP. *Radiocarbon* 55, 1869–1887.
774 https://doi.org/10.2458/azu_js_rc.55.16947

775 Riebe, C.S., Kirchner, J.W., Finkel, R.C., 2004. Erosional and climatic effects on long-term chemical weathering
776 rates in granitic landscapes spanning diverse climate regimes. *Earth and Planetary Science Letters* 224,
777 547–562. <https://doi.org/10.1016/j.epsl.2004.05.019>

778 Rodés, Á., 2008. La última deglaciación en los pirineos: de superficies de exposición mediante ^{10}Be , y modelado
779 numérico de paleoglaciares (<http://purl.org/dc/dcmitype/Text>). Universitat de Barcelona.

780 Schaller, M., Ehlers, T.A., Blum, J.D., Kallenberg, M.A., 2009. Quantifying glacial moraine age, denudation, and
781 soil mixing with cosmogenic nuclide depth profiles. *Journal of Geophysical Research: Earth Surface* 114.
782 <https://doi.org/10.1029/2007JF000921>

783 Stone, J.O., 2000. Air pressure and cosmogenic isotope production. *Journal of Geophysical Research: Solid*
784 *Earth* 105, 23753–23759. <https://doi.org/10.1029/2000JB900181>

785 Stübner, K., Grin, E., Hidy, A.J., Schaller, M., Gold, R.D., Ratschbacher, L., Ehlers, T., 2017. Middle and Late
786 Pleistocene glaciations in the southwestern Pamir and their effects on topography. *Earth and Planetary*
787 *Science Letters* 466, 181–194. <https://doi.org/10.1016/j.epsl.2017.03.012>

788 Sumner, P., Nel, W., 2002. The effect of rock moisture on Schmidt hammer rebound: tests on rock samples
789 from Marion Island and South Africa. *Earth Surface Processes and Landforms* 27, 1137–1142.
790 <https://doi.org/10.1002/esp.402>

791 Tomkins, M.D., Huck, J.J., Dortch, J.M., Hughes, P.D., Kirkbride, M.P., Barr, I.D., 2018a. Schmidt Hammer
792 exposure dating (SHED): Calibration procedures, new exposure age data and an online calculator.
793 *Quaternary Geochronology* 44, 55–62. <https://doi.org/10.1016/j.quageo.2017.12.003>

794 Tomkins, M.D., Dortch, J.M., Hughes, P.D., Huck, J.J., Stimson, A.G., Delmas, M., Calvet, M., Pallàs, R., 2018b.
795 Rapid age assessment of glacial landforms in the Pyrenees using Schmidt hammer exposure dating (SHED).
796 *Quaternary Research* 90, 26–37. <https://doi.org/10.1017/qua.2018.12>

797 Tylmann, K., Woźniak, P.P., Rinterknecht, V.R., 2018. Erratics selection for cosmogenic nuclide exposure
798 dating - an optimization approach. *Baltica* 31, 100–114. <https://doi.org/10.5200/baltica.2018.31.10>

799 Williams, R.B.G., Robinson, D.A., 1983. The effect of surface texture on the determination of the surface
800 hardness of rock using the schmidt hammer. *Earth Surface Processes and Landforms* 8, 289–292.
801 <https://doi.org/10.1002/esp.3290080311>

802 Zech, R., Glaser, B., Sosin, P., Kubik, P.W., Zech, W., 2005. Evidence for long-lasting landform surface
803 instability on hummocky moraines in the Pamir Mountains (Tajikistan) from ^{10}Be surface exposure dating.
804 *Earth and Planetary Science Letters* 237, 453–461. <https://doi.org/10.1016/j.epsl.2005.06.031>

805 Zreda, M.G., Phillips, F.M., 1995. Insights into alpine moraine development from cosmogenic ^{36}Cl buildup
806 dating. *Geomorphology, Glacial Geomorphology: Process and Form Development* 14, 149–156.

807 [https://doi.org/10.1016/0169-555X\(95\)00055-9](https://doi.org/10.1016/0169-555X(95)00055-9)

808 Zreda, M.G., Phillips, F.M., Elmore, D., 1994. Cosmogenic ^{36}Cl accumulation in unstable landforms: 2.
809 Simulations and measurements on eroding moraines. *Water Resources Research* 30, 3127–3136.

810 <https://doi.org/10.1029/94WR00760>

811